Enhanced Oxygen Mobility and Reactivity for Ethanol Steam Reforming

Chengxi Zhang, Shuirong Li, Maoshuai Li, Shengping Wang, Xinbin Ma and Jinlong Gong
Key Laboratory for Green Chemical Technology of Ministry of Education, School of Chemical Engineering and Technology, Tianjin University, Tianjin 300072, P.R. China

DOI 10.1002/aic.12599
Published online March 31, 2011 in Wiley Online Library (wileyonlinelibrary.com).

This article describes a strategy for increasing oxygen storage capacity (OSC) of ethanol steam reforming (ESR) catalysts. Sintering and carbon deposition are major defects of nickel-based catalysts for ESR; tuning oxygen mobility (OM) of CeO_2-based supports can overcome these drawbacks and promote H_2 production. We have successfully increased OSC and OM by adding Mg into the lattice of Ni/CeO_2 to promote H_2 production in ESR. The insertion of Mg into the CeO_2 lattice efficiently promotes the reduction of Ce^{4+} according to X-ray powder diffraction (XRD) and temperature-programmed reduction (TPR) analysis. Mg-modified Ni/CeO_2 catalysts have larger OSC and smaller nickel crystallite size compared with bare Ni/CeO_2. The optimal Mg addition is 7 mol % (Ni/7MgCe) with the best OM. We also present evidence indicating that Mg addition significantly promotes ethanol conversion and H_2 production in ESR, and that Ni/7MgCe yields the best performance due to the high OM of the support. These Mg-modified catalysts also produce less carbon deposition compared with Ni/CeO_2, and the amount of deposited carbon decreases with increasing Mg addition. Ni/7MgCe has the best resistance to carbon deposition owing to the excellent OM. *AIChE J,* 58: 516–525, 2012
Keywords: ethanol steam reforming, hydrogen production, oxygen mobility, Ni/CeO_2, Mg addition

Introduction

Energy is an indispensable element in our everyday lives. Nowadays most of the energy we use comes from fossil fuels—a nonrenewable and unclean energy source. Therefore, it is vital for us to explore renewable and clean energy.[1] Hydrogen has been regarded as an ideal fuel to support energy development because of its cleanness and high combustion efficiency.[2] Among numerous approaches for producing hydrogen, steam reforming is a classical and efficient method. Recently, bioethanol steam reforming for hydrogen production has received increasing attention as bioethanol is renewable, cheap, easy to handle, low in toxicity, and thermodynamically feasible to decompose.[3]

Increasing interests in developing hydrogen fuel cells spur investigations on understanding physicochemical properties of ethanol steam reforming (ESR) catalysts. The ESR catalysts mainly include supported base-metals (e.g., Ni, Co, Cu)[4–7] and supported noble metals (e.g., Pt, Rh, Ru, Pd, and Ir)[8–11]. Although noble metal-based catalysts show outstanding activity and stability in ESR,[12,13] their large-scale application is limited primarily due to the high cost. Thus, development of a nonprecious catalytic system with high activity and stability would be an important step in making the ESR economically feasible. Among supported base metals, Ni-based catalysts are excellent candidates for ESR because of the intrinsic activity of nickel in C—C and C—H bond cleavages.[14] However, one of major problems

Correspondence concerning this article should be addressed to X. Ma at xbma@tju.edu.cn or J. Gong at jlgong@tju.edu.cn.

of Ni-based catalysts is sintering of Ni particles and carbon deposition.[15]

CeO_2 has been widely applied in many reactions, including NO_x reduction,[16] water gas shift reaction (WGSR)[17] and steam reforming,[18] owing to its excellent redox property resulted from high oxygen storage capacity (OSC).[19] The mobile oxygen released from the lattice can efficiently oxidize deposited carbon and subsequently resist coke formation on the catalyst surface.[20] The mobile oxygen can also activate water[21] (e.g., forming hydroxyls), leading to a high hydrogen yield in steam reforming reactions.[22] Oxygen mobility (OM) of CeO_2-based support depends on both OSC and Ce redox rate.[23] However, Ce is easy to be oxidized; thus a number of studies have been performed to improve its capability for reduction. Previous studies have reported that the addition of a second metal ion can enhance the Ce reducibility. For a fixed dopant level or oxygen vacancy concentration, the reduction of cerium is more favorable for larger dopant ions, and the enhancement is more pronounced for divalent dopants.[24]

CeO_2-based support has been widely investigated for ESR, and increasing attention has been attracted regarding the role of OSC in improving the catalytic activity by preventing particles from sintering and suppressing carbon deposition. Biswas et al. studied Zr-modified Ni/CeO_2 catalysts, and found that the excellent activity of 30 wt % Ni/$Ce_{0.74}Zr_{0.26}O_2$ could be resulted from the high OSC of the $Ce_{0.74}Zr_{0.26}O_2$ with increased availability of surface oxygen.[25] Djinović et al. examined CuO-CeO_2 catalyst for high-temperature ESR and concluded that the enhanced OM positively influenced performance of the materials of interest.[6] Shi et al. found that nickel particles supported on composite supports (e.g., Ni/MgO-CeO_2) exhibited better performance than those on single supports (e.g., Ni/CeO_2).[26] Although most of these studies mainly focus on qualitatively optimizing CeO_2-based catalysts to promote ESR, the optimal amount of doping metal and the correlation between OM of the support and the ESR activity are less evaluated.

This article describes a strategy of increasing oxygen storage capacity (OSC) of Ni/CeO_2 catalysts by addition magnesium to obtain enhanced reactivity of ESR. We have prepared a series of Mg-modified CeO_2 by citric acid sol–gel method. Ni particles were loaded by impregnation method. The catalysts were characterized by N_2 adsorption/desorption, X-ray powder diffraction (XRD), transmission electron microscopy (TEM), temperature-programmed reduction (TPR), O_2 volumetric chemisorption and thermo gravimetric analysis (TGA). Our results indicate that an appropriate amount of Mg addition (e.g., 7 mol %) can significantly increase the OM of CeO_2, which has a promotional effect on hydrogen production.

Experimental

Catalysts preparation

Mg-modified CeO_2 support was prepared by a citric acid sol–gel method with magnesium nitrate and cerium nitrate as metal precursors. Typically, appropriate amounts of $Mg(NO_3)_2{\cdot}6H_2O$ and $Ce(NO_3)_3{\cdot}6H_2O$ were dissolved in an excess amount of deionized water (i.e., solution of metal nitrate precursors is not saturated). Citric acid with a molar ratio of (Mg+Ce) to citric acid equal to 1 was subsequently dissolved in the prepared solution; which was then evaporated at 60°C using a vacuum rotary until canary sol was formed. The sol was dried at 120°C for 20 h, and was calcined at 600C for 2 h, yielding Mg-Ce oxide supports. Mg loading is 0 mol %, 3 mol %, 5 mol %, 7 mol %, 10 mol %, 50 mol %, and 100 mol %, which are denoted as CeO_2, 3MgCe, 5MgCe, 7MgCe, 10MgCe, 50MgCe, and MgO, respectively.

Ni/MgO-CeO_2 catalysts were prepared by the incipient wetness impregnation method. The prepared supports were impregnated in $Ni(NO_3)_2{\cdot}6H_2O$ ethanol solutions by mechanical agitation at 50°C for 12 h, followed by evaporated at 60°C using vacuum rotary until the ethanol was removed. The resultant solid was dried at 100°C for 12 h, and then calcined at 600°C for 2 h. The amount of Ni loading was fixed to 10 wt %. The as-prepared catalysts are denoted as Ni/CeO_2, Ni/3MgCe, Ni/5MgCe, Ni/7MgCe, Ni/10MgCe, Ni/50MgCe, and Ni/MgO.

Catalyst characterization

Textual properties of the catalysts were measured using a Micromeritics Tristar 3000 analyzer by nitrogen adsorption at the boiling temperature of liquid nitrogen. Before analysis, the samples were degassed at 300°C for 4 h in vacuum. The specific surface areas were calculated from the isotherms using the BET method, and the cumulative volumes of pores were obtained by the BJH method from the desorption branches of the adsorption isotherms.

XRD measurements were performed using a Rigaku C/max-2500 diffractometer employing the graphite filtered Cu Kα radiation (λ= 1.5406 Å). Data were collected over a 2θ range of 15–85° using a scanning rate of 0.02°/step and a scanning time of 1 s/step. The Scherrer equation was used to estimate the mean crystallite size based on the (111) facet of Ni particles.

TEM was conducted to examine the morphology of catalysts employing a FEI Tecnai G2 F20 transmission electron microscope at 100 kV. The sample powder was dispersed in ethanol by sonification; drops of the suspension were applied onto a copper grid-supported transparent carbon foil and dried in air.

TPR was conducted to determine the reduction behavior of the catalysts. The experiments were performed on a Micromeritics AutoChem 2910 TPD/TPR apparatus using 0.1 g of catalyst and a temperature range from 50 to 1000°C at a rate of 10°C/min. A flow rate of 30 mL/min of 10 vol % H_2/Ar was used for the reduction. A thermal conductivity detector (TCD) was employed to determine the amount of hydrogen consumed.

O_2 volumetric chemisorption was conducted at 400°C using a Micromeritics AutoChem 2910 TPD/TPR system. The sample (0.1 g) was first pretreated under flowing Ar (30 mL/min) at 400°C for ~30 min. Injection pulses of H_2 (1.0760 mL) every 2 min up to a maximum reduction of the sample (about 10 pulses) was followed by injection pulses of O_2 (1.0760 mL) every 2 min until the consumption peaks became stable. OSC was calculated based on O_2 uptake. This value characterizes the total amount of oxygen available in

Table 1. Textual Properties of Ni/MgO-CeO_2 Catalysts

Sample	BET Surface Area (m^2/g)	Pore Volume (cm^3/g)	Average Pore Size (nm)	Cell Parameter of CeO_2 in Supports (Å)[1]	Crystallite Size (nm)[2]
Ni/CeO_2	31	0.14	11	5.427	19.5
Ni/3MgCe	41.9	0.16	10.1	5.421	15.9
Ni/5MgCe	43.4	0.14	8.9	5.419	13.5
Ni/7MgCe	43.7	0.16	9.5	5.418	8.7
Ni/10MgCe	44.6	0.14	8.2	5.417	–
Ni/50MgCe	53.7	0.19	9	5.410	–
Ni/MgO	67.8	0.36	16	–	–

[1]Calculated from (111), (200), (220), and (113) facets of the fluorite phase based on XRD patterns.
[2]Calculated from the Ni(111) facet in XRD patterns of Ni/MgO-CeO_2 catalysts using the Scherrer equation.

the oxide.[27] To simulate the cyclical oxygen activity, the above injection process was repeated. The oxygen reuptake was used to characterize the OM in the oxide, which is more representative of the pool of available surface sites for oxygen transfer during actual operation of the catalysts.[28] OSC and OM are expressed in mmol O_2/g catalyst from the O_2 consumption (O_2 pulses).

Carbon deposition analysis was carried out using a thermal analysis system (DTG-50/50H, Shimadzu Corp.). The experiments were performed in a flow of air (30 mL/min) with a heating rate of 10 °C/min and a final temperature of 900°C.

Activity test

Catalytic tests were conducted at the atmospheric pressure in a quartz fixed-bed reactor loaded with 0.2 g catalyst mixed with 1 mL quartz particles. Before the test, the catalysts were reduced at 500°C in situ for 1 h in a flow of 10 vol % H_2/N_2 (50 mL/min). The liquid solution with a water/ethanol molar ratio of 8 was fed at 0.02 mL/min (or 0.06 mL/min) through an HPLC pump into a heated chamber (150°C) to evaporate the solution completely in the stream of N_2 (60 mL/min). The products were analyzed online by two gas chromatographs. One is equipped with a FID, and a Porapak-Q column with N_2 as the carrier gas to analyze the organic species such as ethanol, ethylene, ethane, acetone, and acetaldehyde. The other one is integrated with a TCD and a TDX-01 column using He as the carrier gas to monitor the incondensable gas species including hydrogen, carbon dioxide, carbon monoxide and methane.

Conversion rate of ethanol (X_{EtOH}) is defined as:

$$X_{EtOH} = \frac{F_{EtOH,in} - F_{EtOH,out}}{F_{EtOH,in}} \times 100\%$$

Selectivity of H_2 production (S_{H_2}) is defined as the molar fraction of H_2 produced out of the total hydrogen-based compounds in the products. Selectivities of by-products (S_{CO}, S_{CO_2}, S_{CH_4}, S_{C_2H4}, S_{C_2H6}, S_{CH_3CHO}, S_{CH_3COCH3}) are defined as the mole ratios of the specified component in the outlet gas to the total carbon-based compounds in the product, accounting for stoichiometry. The following equations present the calculations of these selectivities:

$$S_{H_2} = 100 \times \left(\frac{2(\%H_2)}{2(\%H_2) + 4(\%CH_4) + 4(\%C_2H_4) + 6(\%C_2H_6) + 4(\%CH_3CHO) + 6(\%CH_3COCH_3)} \right)$$

$$S_j = 100 \times \left(\frac{(\%j) \times i}{(\%CO) + (\%CO_2) + (\%CH_4) + 2(\%C_2H_4) + 2(\%C_2H_6) + 2(\%CH_3CHO) + 3(\%CH_3COCH_3)} \right)$$

j represents the carbon containing species in the products, including CO, CO_2 CH_4, C_2H_4, C_2H_6, CH_3CHO, and CH_3COCH_3. i is the number of carbon atomics in the carbon containing species.

Results

Textural analyses

Table 1 summarizes textual properties of the Ni/MgO-CeO_2 catalysts. The specific surface area of the Mg-modified catalysts is larger than that of Ni/CeO_2, which increases with increasing Mg addition. The pore volume of the Mg-modified catalysts with Mg addition below 10 mol % is comparable to that of Ni/CeO_2. For Mg addition above 10 mol %, the pore volume increases as Mg addition is increased. Furthermore, all the Mg-modified catalysts are mesoporous materials with average pore sizes of around 10 nm, similar to Ni/CeO_2.

XRD

XRD patterns of the prepared supports are presented in Figure 1. For CeO_2, diffraction peaks (2θ = 28.5°, 33.1°, 47.5°, and 56.3°) are attributed to the (111), (200), (220), and (311) planes of the cubic fluorite structure of CeO_2, respectively. No diffraction peaks for MgO were found when the loading amount of MgO is less than 50 mol %, implying that Mg is well dispersed on CeO_2 or Mg incorporates into the CeO_2 lattice.[29,30] In addition, the cell parameters

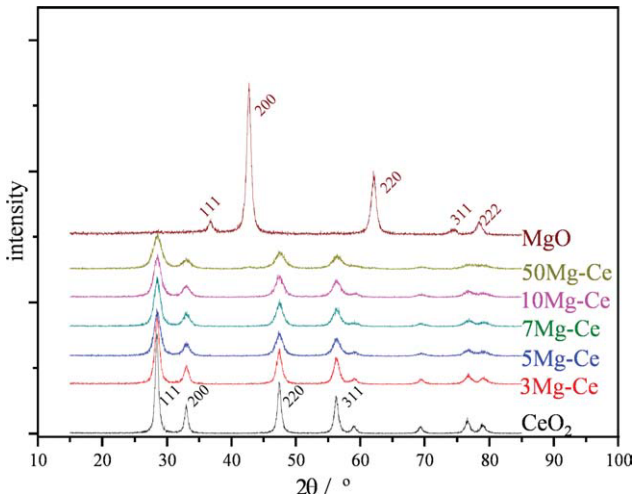

Figure 1. XRD patterns of MgO-CeO_2 supports.

[Color figure can be viewed in the online issue, which is available at wileyonlinelibrary.com.]

(Table 1) of CeO_2 acquired from the XRD spectra decreases with increasing Mg addition.

Nickel-loaded catalysts share similar XRD patterns with the support, except for weak peak intensities of nickel and $Ni_xMg_{1-x}O_2$ solid solution phase (Figure 2). As listed in Table 1, the crystallite sizes of nickel in the catalysts decrease with increasing Mg addition, but there are no nickel diffraction peaks observed when the magnesium loading is greater than 10 mol %. There are two possible explanations, either nickel is well dispersed on the support, or the amount of nickel is beyond the XRD detection limit.[31] On the addition of Mg, the $Ni_xMg_{1-x}O_2$ phase appears, and as expected its intensity increases as Mg loading increases.

TEM

TEM micrographs of the prepared catalysts are shown in Figure 3. Clearly, spherical nickel particles are well dispersed over CeO_2 (Figure 3a). Nickel particles in Ni/CeO_2 have a larger mean particle size (~15 nm) compared with Ni/7MgCe (~7 nm), which is consistent with the results obtained from the XRD spectra. This is probably due to the stronger interaction between Ni and MgO leading to high dispersion of nickel particles.

TPR

TPR profiles of the prepared supports are shown in Figure 4. Bare CeO_2 exhibits two broad reduction peaks. The low temperature (T_L) peak is attributed to the reduction of surface oxygen of CeO_2, and the high temperature (T_H) one is ascribed to the reduction of bulk CeO_2 phase.[32] No reduction peaks were observed for MgO indicating poor reducibility of MgO.[33,34] The intensity of the T_L peak increases with increasing Mg addition, while the T_H peak follows an opposite trend. This phenomenon indicates that the amount of surface oxygen of CeO_2 increases on Mg addition, due to the diffusion of bulk oxygen to the surface accompanying with the Ce^{4+} reduction. Another phenomenon we notice is that the T_L temperature increases with increasing Mg addition whereas the T_H temperature decreases. There is an exception that the T_L temperature of 7MgCe is lower than that of any other supports. This indicates that an optimal loading amount of Mg is 7 mol % which greatly promotes the Ce^{4+} reduction.

We also examine the TPR property of Ni/MgO-CeO_2 catalysts for comparison purpose (Figure 5). The Ni/MgO catalyst has two reduction peaks, the first one centered at 400°C is attributed to the reduction of bulk NiO and the second one centered at 800°C is attributed to the reduction of $Ni_xMg_{1-x}O_2$ solid solution.[35] The intensity of the second peak is stronger than the first one, suggesting that most nickel forms $Ni_xMg_{1-x}O_2$ solid solution as nickel strongly interacts with MgO. Ni/CeO_2 catalysts exhibit four reduction peaks, which are marked as T_1, T_2, T_3, and T_4. The T_1 and T_2 peaks are considered as a result of the reduction of the adsorbed surface oxygen based on observations by Shen and coworkers.[36,37] T_3 is attributed to the reduction of the bulk NiO and the surface CeO_2, and T_4 to the reduction of the bulk CeO_2. The intensity of the T_3 peak decreases with increasing Mg addition, and the corresponding temperature shifts to higher values, because the addition of Mg could weaken the reducibility of Ni species.[38]

OSC and OM

Table 2 lists results obtained from oxygen volumetric chemisorption measurements. It is apparent that Mg-modified CeO_2 support has larger OSC than CeO_2, and 5MgCe has the best OSC, which indicates that Mg addition increases the amount of oxygen vacancies in CeO_2 lattice. Additionally, cyclical oxygen activity test reveals that only 7MgCe shows considerable oxygen uptake, while other supports consume almost no oxygen, indicating that the highest mobility of oxygen on 7MgCe.

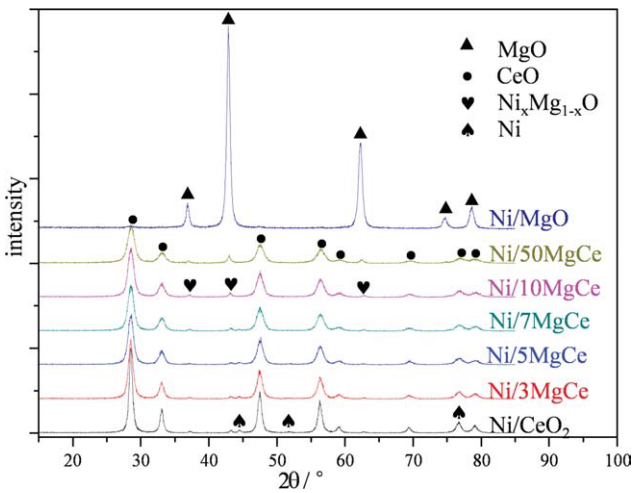

Figure 2. XRD patterns of Ni/MgO-CeO_2 catalysts after 1 h reduction at 500°C.

[Color figure can be viewed in the online issue, which is available at wileyonlinelibrary.com.]

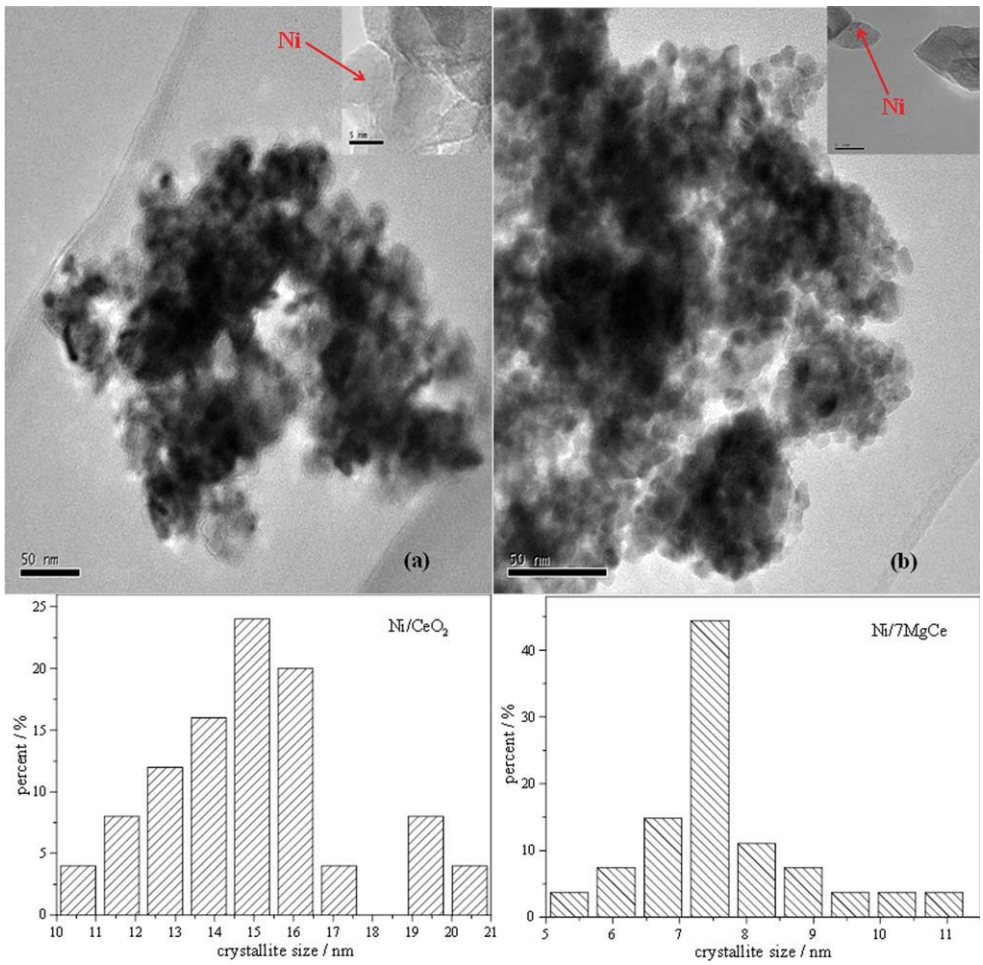

Figure 3. TEM micrographs and crystallite size distribution of the prepared catalysts after 1 h reduction: (a) Ni/CeO_2; (b) Ni/7MgCe.

[Color figure can be viewed in the online issue, which is available at wileyonlinelibrary.com.]

Catalytic activities

Ethanol conversion and selectivities of products on the Ni/MgO-CeO_2 catalysts are illustrated in Figure 6. The major products are H_2, CO, CO_2, and CH_4 for all the studied catalysts, and the C2 and C3 (e.g., C_2H_4, C_2H_6, CH_3CHO, and CH_3COCH_3) species are only produced when Mg addition is larger than 7 mol %. Ethanol conversion remained 100 % unless Mg addition is larger than 10 mol %, above which conversion decreases drastically from 100 % to 20 %. Selectivities of H_2, CO, and CO_2 increase with increasing Mg addition when Mg addition is less than 10 mol %, whereas CH_4 selectivity decreases.

ESR on Ni/7MgCe and Ni/10MgCe were conducted at various conditions to further address the effect of addition of Mg (Figure 7). On decreasing the space time to 11 g h/mol (Figure 7a), ethanol was not completely converted. Ethanol conversion and H_2 selectivity over Ni/7MgCe were higher compared with Ni/10MgCe, which, in turn, had a higher C2 and C3 selectivity. Increasing the reaction temperature from 400°C to 600°C has negligible effect on ethanol conversion (Figure 7b), whereas H_2 and CO_2 selectivities over Ni/7MgCe are higher than that of Ni/10MgCe. We also notice higher selectivity of by-products (e.g., CH_4, C2 and C3species) formed on Ni/10MgCe compared with Ni/7MgCe, further indicating the optimal Mg addition of 7 mol %.

Carbon deposition

We observed the deactivation of the catalysts as reaction proceeds (e.g., after 10 h), due to the formation of coke. The nature of deposited carbon was therefore studied by TGA (Figure 8). The amount of carbon deposited on the catalysts decreases as Mg addition increases. The weight losses of the catalysts based on TGA results occurred at 600°C (not shown in the figure) attributed to graphite carbon.[29,39] Because most carbon is deposited on nickel surface,[40] carbon deposition per unit Ni (i.e., the amount of carbon deposition divided by the amount of reducible Ni) of the catalysts is shown in the inset of Figure 8. It is apparent that Ni/7MgCe has the least carbon deposition among the catalysts with excellent reactivity (Mg addition less than 10 mol %). Note that Ni/50MgCe and Ni/MgO have less carbon deposition simply because of their low reaction activity.

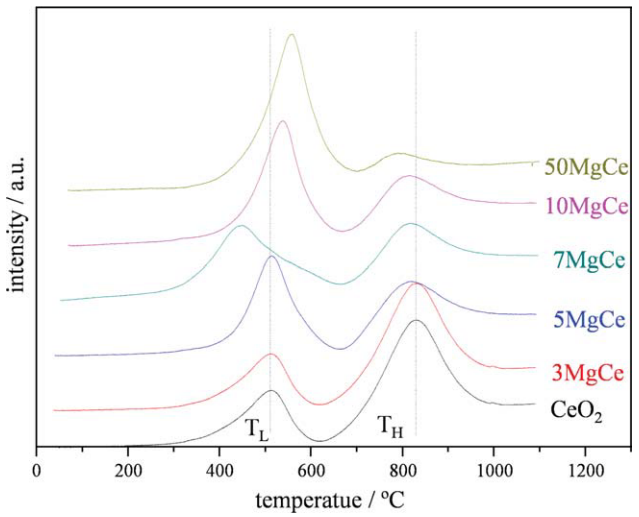

Figure 4. TPR profiles of MgO-CeO_2 supports.

[Color figure can be viewed in the online issue, which is available at wileyonlinelibrary.com.]

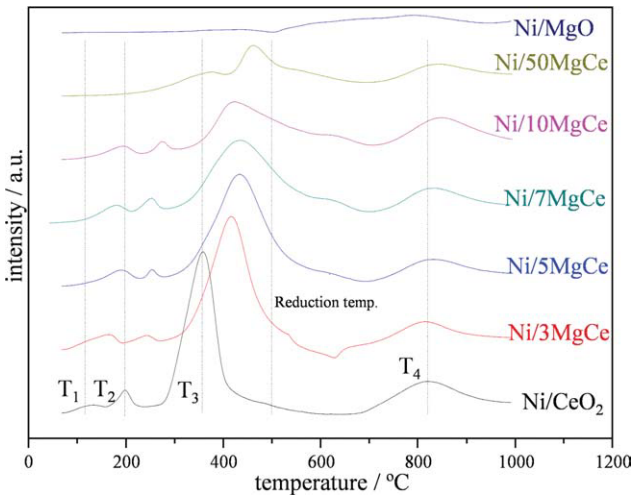

Figure 5. TPR profiles of Ni/MgO-CeO_2 catalysts.

[Color figure can be viewed in the online issue, which is available at wileyonlinelibrary. com.]

Discussions

Supports

Ceria easily forms solid solutions with transition-metal/rare-earth oxides over a wide composition range. There are two types of substitutions when the metal is incorporated into the CeO_2 support. When the metal ion has an ionic radius similar to that of the host (e.g., Ce^{4+}: 97 pm),[41] it can occupy the Ce^{4+} sites by isomorphous substitution. However, if the metal ion has a much smaller ionic radius, it would occupy defect sites or surface vacancies of the CeO_2 crystals. It has been proved that Zr^{4+} could substitute Ce^{4+} and form the $Ce_xZr_{1-x}O_2$ solid solutions as Zr^{4+} is a homovalent ion compared with Ce^{4+}.[42–44] Hong et al. examined physical properties of CeO_x-MnO_y support and found that the ionic radius of Mn^{2+} was similar to that of Ce^{4+} and occupied Ce^{4+} sites by substitution, whereas Mn^{3+} occupied defect sites of CeO_2 owing to its much smaller ionic radius.[45] Mg^{2+} has an ion radius of 89 pm,[41] which is a little smaller than that of Ce^{4+}, so it can substitute Ce^{4+} or occupy the defect sites in the CeO_2 crystal. As cell parameters of CeO_2 decrease with increasing Mg addition according to XRD results, it suggests that Mg^{2+} has substituted Ce^{4+} and forms a small amount of nonequilibrium $Mg_xCe_{1-x/2}O_2$ solid solution.[46,47]

Doped-ceria with metal ions can modify OSC and OM of the support by lowering the barrier for oxygen migration and decreasing the activation energy for the reduction ($Ce^{4+} \rightarrow Ce^{3+}$).[48] When a Ce^{4+} ion is substituted with a metal ion, an oxygen vacancy is formed to maintain the charge balance, while metal ion in defect or surface sites cause the disappearance of oxygen vacancies. The formation of oxygen vacancy will consequently lower the energy of oxygen migration and increase OSC of the support, and if Ce^{4+} reduction is promoted, OM of the support would be enhanced. From OSC data, we have learned that Mg-modified CeO_2 support has larger OSC than CeO_2, and 5 mol % addition has the largest OSC; on further adding Mg, the OSC decreases. Therefore, there could be a maximum in the substitution of Ce^{4+} by Mg^{2+}, and excessive Mg^{2+} would occupy some of the defect sites of the CeO_2 crystal, leading to a decrease in OSC. Hong et al. found that a limited amount of Mn addition would increase OSC of the support, but a further increase Mn decreased the concentration of oxygen vacancies of the support.[45] Deshpande et al. studied noble-metal-substituted ceria and found that a proper amount of Pt substitution could increase OSC of the catalyst.[49] In our case, Mg addition with 7 mol % greatly promotes Ce^{4+} reduction according to TPR analysis, and OSC test demonstrates the highest OM of the 7MgCe support. Reddy et al. adopted La substitution into CeO_2 lattice, and found that $Ce_{1-x}La_xO_{2-\delta}$ ($x = 0.2$) had an excellent reducibility and OM.[50] Mg can incorporate into the CeO_2 lattice and increase the OSC of the support; an appropriate amount of Mg addition greatly promotes the Ce^{4+} reduction, and thus enhances the OM of the support.

Nickel catalysts

The addition of magnesium not only increases OSC of the support, but also makes modification on nickel particles.

Table 2. Oxygen Storage Capacity of MgO-CeO_2 Supports

	Oxygen Storage Capacity (mmol/g)						
Number of Times[1]	CeO_2	3MgCe	5MgCe	7MgCe	10MgCe	50MgCe	MgO
1	1.06	5.28	8.54	5.86	2.17	2.01	0.68
2	0.017	0.027	0.043	4.81	0.034	0.004	0.11

[1]The first time OSC indicates the total OSC, and the second time OSC refers to the OM.

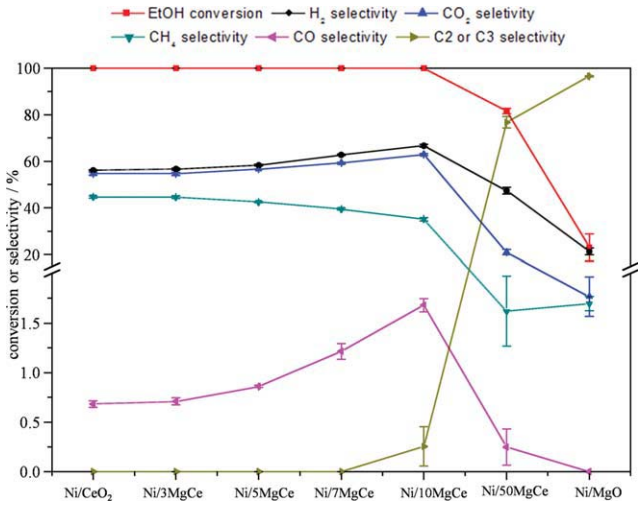

Figure 6. Ethanol steam reforming on Ni/MgO-CeO_2 catalysts.

Reaction conditions: Pressure: 1 atm, temperature: 400°C, S/C: 4, Ethanol feeding W/F: 33 g h/mol. [Color figure can be viewed in the online issue, which is available at wileyonlinelibrary.com.]

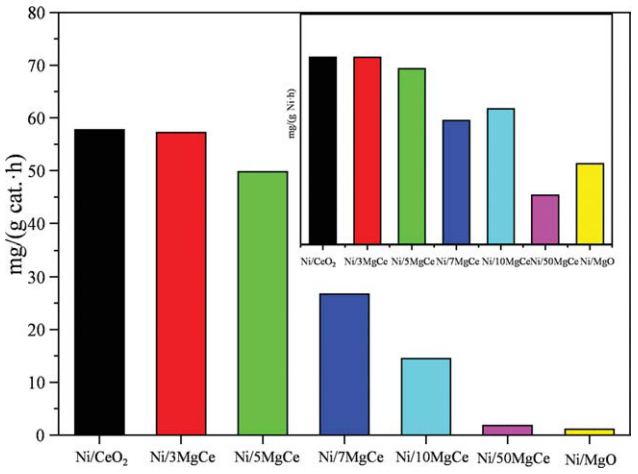

Figure 8. Carbon depositions on the Ni/MgO-CeO_2 catalysts after 10-h reaction (reaction conditions: 1 atm, 400°C, and ethanol feeding W/F 33 g h/mol); inset: carbon deposition per unit Ni on the Ni/MgO-CeO_2 catalysts.

[Color figure can be viewed in the online issue, which is available at wileyonlinelibrary.com.]

Areas of the peaks in TPR profiles were integrated and the results are listed in Table 3. Because the reduction temperature employed in this work is 500°C, the involved reduction peaks are T_L, T_1, T_2, and T_3. The portion of reducible Ni is calculated as $(T_1 + T_2 + T_3 - T_L)$, as also reported earlier by Biswas.[25] Obviously the amount of reducible Ni decreases with increasing Mg addition. This could be caused by the strong interaction between NiO and MgO evidenced by the formation of the $Ni_xMg_{1-x}O_2$ solid solution,[51] as confirmed by our XRD results. This characteristic can also explain the inhibition of the sintering of Ni during the calcination and the reduction processes, as confirmed by our TEM results. Indeed, earlier investigations have implied the poor reducibility of nickel on MgO and the inhibition of nickel sintering by Ni/Mg interaction.[35,38,52,53]

Reaction analysis

In the ESR process, main reactions are as follows:[54,55]

$$C_2H_5OH \rightarrow CH_3CHO + H_2 \quad (1)$$

$$CH_3CHO \rightarrow CO + CH_4 \quad (2)$$

$$CO + H_2O \leftrightarrow CO_2 + H_2 \quad (3)$$

$$CH_4 + xH_2O \leftrightarrow CO_x + (x+2)H_2 \quad (4)$$

In this system, nickel primarily promotes C—C and C—H cleavages [reactions (1) and (2)]. Nickel particles also have activity in CH_4 and CO transformation [reactions (3) and (4)].[4] As both reactions are reversible, different conditions

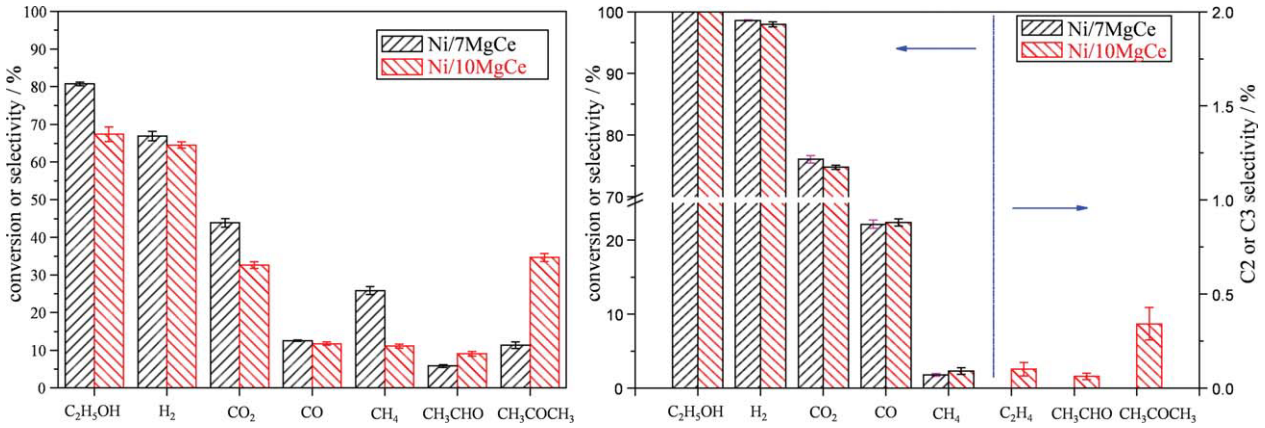

Figure 7. Ethanol steam reforming on Ni/7MgCe and Ni/10MgCe at different reaction conditions.

(a) Pressure: 1 atm, temperature: 400°C, S/C:4, ethanol feeding W/F:11 g h/mol; (b) Pressure: 1 atm, temperature: 600°C, S/C: 4, ethanol feeding W/F: 33 g h/mol. [Color figure can be viewed in the online issue, which is available at wileyonlinelibrary.com.]

Table 3. Peak Areas Integrated from TPR Profiles

Catalyst	Area T_L	Area T_1	Area T_2	Area T_3	Reducible Ni[1]	Portion of Reducible Ni (%)[2]
Ni/CeO_2	1.8	0.1	0.4	10.3	9.0	100
Ni/3MgCe	2.0	0.4	0.2	10.2	8.8	98
Ni/5MgCe	3.0	0.5	0.1	10.6	8.2	91
Ni/7MgCe	3.1	0.5	0.3	8.6	6.3	70
Ni/10MgCe	3.5	0.4	0.2	6.0	3.1	34
Ni/50MgCe	4.4	–	1.6	3.9	1.1	12
Ni/MgO	–	–	–	0.4	0.4	5

[1]Calculated by $(T_1 + T_2 + T_3) - T_L$.
[2]Portion of reducible Ni in Ni/CeO_2 is 100%.

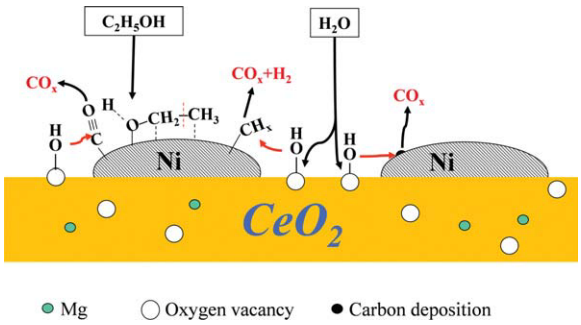

Figure 9. Proposed reaction scheme of ethanol steam reforming on Ni/MgO-CeO_2 catalysts.

[Color figure can be viewed in the online issue, which is available at wileyonlinelibrary.com.]

could induce different products distributions. From Figure 6, we can see that CO is traceable on all the studied catalysts at 400°C, owing to the high OM of CeO_2-based supports.[19] It turns out that CeO_2 can also promote methane steam reforming primarily due to the presence of oxygen vacancies,[56] leading to a decrease in selectivity of CH_4 and thus an increase in selectivities of CO_2 and H_2. Previous studies have proved that nickel had high activity in methanation.[57,58] As methanation is favored under studied condition, the amount of reduced Ni is expected to influence methane selectivity. Therefore, decreasing amount of reducible Ni on Mg addition could cause a decrease in selectivity of CH_4.[59] On the other hand, C2 and C3 species are produced when the amount of Mg addition is larger than 10 mol %, probably due to the deficient ability of C—C cleavage with decreasing amount of nickel in the catalysts. When space velocity rises, this effect would be intensified, and thus ethanol conversion and H_2 selectivity of Ni/7MgCe are higher compared with Ni/10MgCe. At 600°C, both nickel and the support with mobile oxygen species favor CH_4 and CO transformation, resulting in higher selectivities of H_2 and CO_2 on Ni/7MgCe than Ni/10MgCe. In addition, no C2 and C3 products were detected over Ni/7MgCe, whereas C_2H_4, CH_3CHO and CH_3COCH_3 were all produced on Ni/10MgCe.

Highly mobile oxygen species of the support can also suppress carbon deposition.[60] Liu et al. suggested that Ce^{4+} ions on the surface of support can oxidize the deposited coke to form Ce^{3+} ions in the presence of NiP nanoparticles, leading to the formation of oxygen vacancies.[61] da Silva et al. examined the effect of support reducibility on the stability of ESR and concluded that the high oxygen/OH mobility of the CeO_2 support contributed to the high stability and reactivity of the catalyst.[62] Laosiripojana et al. proposed that enhanced redox properties of doped ceria prevented carbon deposition by oxidizing the adsorbed surface hydrocarbons on nickel surface.[63] It turns out that our Ni/7MgCe catalyst has the best OM, coincided with the least carbon deposition per unit Ni.

We should mention that Mg addition not only increases the OSC and the OM of the support, but also decreases the crystallite size of nickel particles. The strong interaction between nickel and the MgO-CeO_2 support can prevent the sintering of nickel particle in the calcination and reduction processes. Based on our results regarding the role of OM, a plausible reaction scheme of ESR is proposed in Figure 9. In the presence of nickel, the first key reaction should be the dehydrogenation of ethanol to surface adsorbed CH_3CHO_{ads}.[4] As Yates and coworkers have shown, metallic nickel particles cause bond breaking of ethanol in the following order: O—H, —CH_2—, C—C, and —CH_3.[14,64] Therefore, the following scheme should be the transformation of CH_3CHO_{ads}. When there is enough nickel in the catalyst (e.g., Ni/7MgCe), C—C cleavage occurs to produce adsorbed C≡O and CH_x on the nickel surface.[65] Otherwise (as in the case of Ni/10MgCe), CH_3CHO_{ads} would be transformed into other oxygenates (e.g., CH_3COCH_3 and CH_3COOH). As nickel has low ability to activate water,[66] water is chemisorbed on vacancies of the CeO_2 surface forming hydroxyls, which migrate through oxygen vacancies on the CeO_2 surface.[67] These oxygen species (including hydroxyls) originating from water can oxidize C≡O and CH_x to form H_2 and CO_x. Therefore, if there is sufficient oxygen species on the catalyst surface, the intermediate products can be fully converted to CO_2 and H_2. However, if OM of the support is poor, consumption rate of oxygen species is slower compared with its forming rate, and a significant amount of byproducts (e.g., CH_4 and carbon) would be formed. The primary role of Mg addition is to increase the amount of oxygen vacancies resulting in an enhancement of the OM of CeO_2-based supports, and thus promote the ESR to produce H_2.

Conclusions

We have presented an investigation into how Mg addition into Ni/CeO_2 can facilitates the formation of mobile oxygen in the catalysts. XRD and TPR analysis displayed that Mg can be incorporated into CeO_2 lattice and promote Ce^{4+} reduction. Mg-modified CeO_2 support has more oxygen vacancies and higher OSC than the bare CeO_2, and the optimized concentration is 7 mol %. Because of the strong interaction between NiO and MgO, the amount of reducible Ni decreases sharply with further increasing Mg addition (e.g., above 10 mol %). Mg-modified catalysts also have better resistance to coke formation compared with Ni/CeO_2, and Ni/7MgCe has the least carbon deposition per unit Ni.

Acknowledgments

The authors acknowledge the financial support from the National Natural Science Foundation of China (21006068, 20936003, 21050110425), the Program for New Century Excellent Talents in University (NCET-

04-0242), Seed Foundation of Tianjin University (60303002), and the Program of Introducing Talents of Discipline to Universities (B06006).

Literature Cited

1. Kothari R, Buddhi D, Sawhney R. Comparison of environmental and economic aspects of various hydrogen production methods. *Renew Sust Energy Rev*. 2008;12:553–563.
2. Agrawal R, Offutt M, Ramage MP. Hydrogen economy—an opportunity for chemical engineers? *AIChE J*. 2005;51:1582–1589.
3. Ni M, Leung DYC, Leung MKH. A review on reforming bio-ethanol for hydrogen production. *Int J Hydrogen Energy*. 2007;32:3238–3247.
4. Fatsikostas AN, Verykios XE. Reaction network of steam reforming of ethanol over Ni-based catalysts. *J Catal*. 2004;225:439–452.
5. Wang H, Liu Y, Wang L, Qin YN. Study on the carbon deposition in steam reforming of ethanol over Co/CeO_2 catalyst. *Chem Eng J*. 2008;145:25–31.
6. Djinović P, Batista J, Ćehić B, Pintar A. Utilization of high specific surface area $CuO–CeO_2$ catalysts for high temperature processes of hydrogen production: steam re-forming of ethanol and methane dry re-forming. *J Phys Chem A*. 2009;114:3939–3949.
7. Tang Y, Liu Y, Zhu P, Xue Q, Chen L, Lu Y. High-performance HTLcs-derived CuZnAl catalysts for hydrogen production via methanol steam reforming. *AIChE J*. 2009;55:1217–1228.
8. Mathure PV, Ganguly S, Patwardhan AV, Saha RK. Steam reforming of ethanol using a commercial nickel-based catalyst. *Ind Eng Chem Res*. 2007;46:8471–8479.
9. Song H, Zhang LZ, Ozkan US. Effect of synthesis parameters on the catalytic activity of $CO-ZrO_2$ for bio-ethanol steam reforming. *Green Chem*. 2007;9:686–694.
10. de Lima SM, da Cruz IO, Jacobs G, Davis BH, Mattos LV, Noronha FB. Steam reforming, partial oxidation, and oxidative steam reforming of ethanol over $Pt/CeZrO_2$ catalyst. *J Catal*. 2008;257:356–368.
11. Can F, Le Valant A, Bion N, Epron F, Duprez D. New active and selective $Rh-ReO_x-Al_2O_3$ catalysts for ethanol steam reforming. *J Phys Chem C*. 2008;112:14145–14153.
12. Breen JP, Burch R, Coleman HM. Metal-catalysed steam reforming of ethanol in the production of hydrogen for fuel cell applications. *Appl Catal B*. 2002;39:65–74.
13. Cavallaro S, Chiodo V, Freni S, Mondello N, Frusteri F. Performance of Rh/Al_2O_3 catalyst in the steam reforming of ethanol: H_2 production for MCFC. *Appl Catal A*. 2003;249:119–128.
14. Gates SM, Russell JN Jr, Yates JT Jr. Bond activation sequence observed in the chemisorption and surface reaction of ethanol on Ni(111). *Surf Sci*. 1986;171:111–134.
15. Sehested J. Four challenges for nickel steam-reforming catalysts. *Catal Today*. 2006;111:103–110.
16. Ilieva L, Pantaleo G, Ivanov I, Venezia AM, Andreeva D. Gold catalysts supported on CeO_2 and $CeO_2-Al_2O_3$ for NO_x reduction by CO. *Appl Catal B*. 2006;65:101–109.
17. Duartedefarias A, Barandas A, Perez R, Fraga M. Water-gas shift reaction over magnesia-modified Pt/CeO_2 catalysts. *J Power Sources*. 2007;165:854–860.
18. Sun J, Wang Y, Li J, Xiao G, Zhang L, Li H, Cheng Y, Sun C, Cheng Z, Dong Z, Chen L. H_2 production from stable ethanol steam reforming over catalyst of NiO based on flowerlike CeO_2 microspheres. *Int J Hydrogen Energy*. 2010;35:3087–3091.
19. Gorte RJ. Ceria in catalysis: from automotive applications to the water-gas shift reaction. *AIChE J*. 2010;56:1126–1135.
20. Profeti LPR, Ticianelli EA, Assaf EM. Production of hydrogen via steam reforming of biofuels on $Ni/CeO_2-Al_2O_3$ catalysts promoted by noble metals. *Int J Hydrogen Energy*. 2009;34:5049–5060.
21. Wang X, Rodriguez JA, Hanson JC, Gamarra D, Martínez-Arias A, Fernández-García M. In situ studies of the active sites for the water gas shift reaction over $Cu–CeO_2$ catalysts: complex interaction between metallic copper and oxygen vacancies of ceria. *J Phys Chem B*. 2005;110:428–434.
22. de Lima SM, da Silva AM, da Costa Loo, Graham UM, Jacobs G, Davis BH, Mattos LV, Noronha FB. Study of catalyst deactivation and reaction mechanism of steam reforming, partial oxidation, and oxidative steam reforming of ethanol over Co/CeO_2 catalyst. *J Catal*. 2009;268:268–281.
23. Liu X, Zhou K, Wang L, Wang B, Li Y. Oxygen vacancy clusters promoting reducibility and activity of ceria nanorods. *J Am Chem Soc*. 2009;131:3140–3141.
24. Balducci G, Islam MS, Kaspar J, Fornasiero P, Graziani M. Reduction process in CeO_2-MO and $CeO_2-M_2O_3$ mixed oxides: a computer simulation study. *Chem Mater*. 2003;15:3781–3785.
25. Biswas P, Kunzru D. Steam reforming of ethanol for production of hydrogen over $Ni/CeO_2–ZrO_2$ catalyst: effect of support and metal loading. *Int J Hydrogen Energy*. 2007;32:969–980.
26. Shi Q, Liu C, Chen W. Hydrogen production from steam reforming of ethanol over $Ni/MgO-CeO_2$ catalyst at low temperature. *J Rare Earth*. 2009;27:948–954.
27. Madier Y, Descorme C, Le Govic AM, Duprez D. Oxygen mobility in CeO_2 and $Ce_xZr_{(1-x)}O_2$ compounds: study by CO transient oxidation and $^{18}O/^{16}O$ isotopic exchange. *J Phys Chem B*. 1999;103:10999–11006.
28. Yao HC, Yao YFY. Ceria in automotive exhaust catalysts. I. Oxygen storage. *J Catal*. 1984;86:254–265.
29. Li M, Wang X, Li S, Wang S, Ma X. Hydrogen production from ethanol steam reforming over nickel based catalyst derived from Ni/Mg/Al hydrotalcite-like compounds. *Int J Hydrogen Energy*. 2010;35:6699–6708.
30. Chen J, Zhu J, Chen C, Zhan Y, Cao Y, Lin X, Zheng Q. Effect of Mg addition on the physical and catalytic properties of Cu/CeO_2 for NO + CO reduction. *Catal Lett*. 2009;130:254–260.
31. Li Y, Guo Y, Xue B. Catalytic combustion of methane over M (Ni, Co, Cu) supported on ceria–magnesia. *Fuel Process Technol*. 2009;90:652–656.
32. Laguna OH, Romero Sarria F, Centeno MA, Odriozola JA. Gold supported on metal-doped ceria catalysts (M = Zr, Zn and Fe) for the preferential oxidation of CO (PROX). *J Catal*. 2010;276:360–370.
33. Arena F, Licciardello A, Parmaliana A. The role of Ni^{2+} diffusion on the reduciablity of NiO/MgO system: a combined TRP-XPS study. *Catal Lett*. 1990;6:139–149.
34. Naito S, Tanaka H, Kado S, Miyao T, Naito S, Okumura K, Kunimori K, Tomishige K. Promoting effect of Co addition on the catalytic partial oxidation of methane at short contact time over a Rh/MgO catalyst. *J Catal*. 2008;259:138–146.
35. Li M, Li S, Zhang C, Wang S, Ma X, Gong J. Ethanol steam reforming over $Ni/Ni_xMg_{1-x}O$: inhibition of surface nickel species diffusion into the bulk. *Int J Hydrogen Energy*. 2010;36:326–332.
36. Zhang B, Tang X, Li Y, Cai W, Xu Y, Shen W. Steam reforming of bio-ethanol for the production of hydrogen over ceria-supported Co, Ir and Ni catalysts. *Catal Commun*. 2006;7:367–372.
37. Shan, W. Reduction property and catalytic activity of $Ce_{1-X}Ni_XO_2$ mixed oxide catalysts for CH_4 oxidation. *Appl Catal A*. 2003;246:1–9.
38. Narayanan S, Sreekanth G. Problems involved in the reducibility of the NiO-MgO system as evidenced by X-ray diffraction, electron paramagnetic resonance, electron spectroscopy for chemical analysis and adsorption techniques. *J Chem Soc Faraday Trans*. 1993;89:943–949.
39. Natesakhawat S, Watson RB, Wang X, Ozkan US. Deactivation characteristics of lanthanide-promoted sol-gel Ni/Al_2O_3 catalysts in propane steam reforming. *J Catal*. 2005;234:496–508.
40. Bartholomew CH. Carbon deposition in steam reforming and methanation. *Catal Rev Sci Eng*. 1982;24:67–112.
41. Shannon RD. Revised effective ionic radii and systematic studies of interatomic distances in halides and chalcogenides. *Acta Crystallogr A*. 1976;32:751–767.
42. Laosiripojana N, Kiatkittipong W, Assabumrungrat S. Partial oxidation of palm fatty acids over $Ce-ZrO_2$: roles of catalyst surface area, lattice oxygen capacity and mobility. *AIChE J*. 2010;36:326–332.
43. Monte RD, Kaspar J. Nanostructured $CeO_2–ZrO_2$ mixed oxides. *J Mater Chem*. 2005;15:633–648.
44. Trovarelli A. Catalytic properties of ceria and CeO_2-containing materials. *Catal Rev Sci Eng*. 1996;38:439–520.
45. Hong W-J, Iwamoto S, Hosokawa S, Wada K, Kanai H, Inoue M. Effect of Mn content on physical properties of CeO_x-MnO_y support and $BaO-CeO_x-MnO_y$ catalysts for direct NO decomposition. *J Catal*. 2010;277:208–216.
46. Chen M, Zheng H, Shi C, Zhou R, Zheng X. Synthesis of nanoparticle Ce-Mg-O mixed oxide as efficient support for methane oxidation. *J Mol Catal A: Chem*. 2005;237:132–136.

47. Chen J, Zhu J, Zhan Y, Lin X, Cai G, Wei K, Zheng Q. Characterization and catalytic performance of Cu/CeO_2 and $Cu/MgO\text{-}CeO_2$ catalysts for NO reduction by CO. *Appl Catal A*. 2009;363:208–215.
48. Trovarelli A. Structural and oxygen storage/release properties of CeO_2-based solid solutions. *Comments Inorg Chem*. 1999;20:263–284.
49. Deshpande PA, Hegde MS, Madras G. A mechanistic model for the water-gas shift reaction over noble metal substituted ceria. *AIChE J*. 2010;56:1315–1324.
50. Reddy BM, Katta L, Thrimurthulu G. Novel nanocrystalline $Ce_{1-x}La_xO_{2-\delta}$ ($x = 0.2$) solid solutions: structural characteristics and catalytic performance. *Chem Mater*. 2009;22:467–475.
51. Nakamura K, Miyazawa T, Sakurai T, Miyao T, Naito S, Begum N, Kunimori K, Tomishige K. Promoting effect of MgO addition to $Pt/Ni/CeO_2/Al_2O_3$ in the steam gasification of biomass. *Appl Catal B*. 2009;86:36–44.
52. Chen Y-g, Tomishige K, Yokoyama K, Fujimoto K. Promoting effect of Pt, Pd and Rh noble metals to the $Ni_{0.03}Mg_{0.97}O$ solid solution catalysts for the reforming of CH_4 with CO_2. *Appl Catal A*. 1997;165:335–347.
53. Nagaoka K, Hashimoto Y, Sato K, Wakatsuki T, Nishiguchi H, Takita Y. Addition of Al_2O_3 or Cr_2O_3 promotes metal reduction in a CoO-NiO-MgO solid solution catalyst for CH_4/H_2O reforming. *Chem Lett*. 2008;37:982–983.
54. Haryanto A, Fernando S, Murali N, Adhikari S. Current status of hydrogen production techniques by steam reforming of ethanol: a review. *Energy Fuel*. 2005;19:2098–2106.
55. Vaidya PD, Rodrigues AE. Insight into steam reforming of ethanol to produce hydrogen for fuel cells. *Chem Eng J*. 2006;117:39–49.
56. Laosiripojana N, Assabumrungrat S. Methane steam reforming over $Ni/Ce\text{-}ZrO_2$ catalyst: Influences of $Ce\text{-}ZrO_2$ support on reactivity, resistance toward carbon formation, and intrinsic reaction kinetics. *Appl Catal A*. 2005;290:200–211.
57. Krämer M, Stöwe K, Duisberg M, Müller F, Reiser M, Sticher S, Maier WF. The impact of dopants on the activity and selectivity of a Ni-based methanation catalyst. *Appl Catal A*. 2009;369:42–52.
58. Andersson MP, Abild-Pedersen F, Remediakis IN, Bligaard T, Jones G, Engbæk J, Lytken O, Horch S, Nielsen JH, Sehested J, Rostrup-Nielsen JR, Nørskov JK, Chorkendorff I. Structure sensitivity of the methanation reaction: H_2-induced CO dissociation on nickel surfaces. *J Catal*. 2008;255:6–19.
59. Hu X, Lu GX. Inhibition of methane formation in steam reforming reactions through modification of Ni catalyst and the reactants. *Green Chem*. 2009;11:724–732.
60. Song H, Ozkan US. Ethanol steam reforming over Co-based catalysts: Role of oxygen mobility. *J Catal*. 2009;261:66–74.
61. Liu L, Hong L. Nickel phosphide catalyst for autothermal reforming of surrogate gasoline fuel. *AIChE J*. 2010.
62. da Silva AM, de Souza KR, Mattos LV, Jacobs G, Davis BH, Noronha FB. The effect of support reducibility on the stability of Co/CeO_2 for the oxidative steam reforming of ethanol. *Catal Today*. 2010.
63. Laosiripojana N, Sangtongkitcharoen W, Assabumrungrat S. Catalytic steam reforming of ethane and propane over CeO_2-doped Ni/Al_2O_3 at SOFC temperature: Improvement of resistance toward carbon formation by the redox property of doping CeO_2. *Fuel*. 2006;85:323–332.
64. Xu J, Zhang X, Zenobi R, Yoshinobu J, Xu Z, Yates JT Jr. Ethanol decomposition on Ni(111): observation of ethoxy formation by IRAS and other methods. *Surf Sci*. 1991;256:288–300.
65. Liberatori JWC, Ribeiro RU, Zanchet D, Noronha FB, Bueno JMC. Steam reforming of ethanol on supported nickel catalysts. *Appl Catal A*. 2007;327:197–204.
66. Comas J, Mariño F, Laborde M, Amadeo N. Bio-ethanol steam reforming on Ni/Al_2O_3 catalyst. *Chem Eng J*. 2004;98:61–68.
67. Fronzi M, Piccinin S, Delley B, Traversa E, Stampfl C. Water adsorption on the stoichiometric and reduced $CeO_2(111)$ surface: a first-principles investigation. *Phys Chem Chem Phys*. 2009;11:9188–9199.

Manuscript received Jan. 6, 2011, and revision received Feb. 15, 2011.